圧縮性遷移境界層における非線形渦動力学の全体シミュレーション

課題責任者
松浦　一雄　　愛媛大学　大学院理工学研究科

著者
松浦　一雄　　愛媛大学　大学院理工学研究科

音速の 5 倍以上の速さを有する極超音速流れが物体回りに形成する粘性境界層流れにおける層流から乱流への遷移過程は、境界層の内部で音速より遅い領域と音速以上の速い領域が混在するなど密度変動や温度変動といった複雑因子が多く、それらの相互作用も多彩となるため、その渦動力学に関する詳細解明が期待されている。本研究では、その層流―乱流遷移がどのような非線形渦動力学プロセスを経て起こるのか、圧縮性 Navier-Stokes 方程式の直接シミュレーションを行い明らかにする。線形固有擾乱や等方的な乱れであるか或いは局所的な乱れであるかといった、遷移過程に影響を与える境界層内外の擾乱を変化させながら、遷移ルートの変化を比較すると同時に遷移境界層に出現して遷移を担う渦の挙動と安定性を解明する。

キーワード：極超音速流れ, 層流―乱流遷移, 表面粗さ, 直接シミュレーション, インターフェース条件

1. はじめに

音速の 5 倍以上の速さを有する極超音速流れが物体回りに形成する粘性境界層流れにおける層流から乱流への遷移過程は、我々が普段経験する低速流れの遷移と比較して、境界層の内部で音速より遅い領域と音速以上の領域が混在するなど密度変動や温度変動といった複雑因子が多く、それらの相互作用も多彩となるため、その渦動力学に関する詳細解明の発展が期待されている。

Mack が示したように、超音速あるいは極超音速では、低速流れでも見られる Tollmien-Schlichting 波に対応する第 1 モードに加えて高次の音響不安定モードが存在する [1]。低速流れにおける斜めの不安定な第 1 モードと対照的に極超音流れ境界層では 2 次元の Mack モードが支配的となる。

これまで線形安定性理論、弱非線形安定性理論、放物化安定性方程式、過渡増幅理論といった様々な安定性解析により遷移過程が調べられてきたが、安定性理論と乱流への遷移には依然としてギャップが存在する。一方で、もし初期条件、境界条件、計算格子や時間刻みが適切に与えられれば、直接シミュレーション（DNS）は Navier-Stokes 方程式を忠実に解析できる。

そこで、本研究では極超音速境界層を容易に乱流に導くとされる縦渦を導入する直接シミュレーション、三次元渦に対する完全非線形擾乱方程式の導出および必要な数値計算法の開発を行った。

2. 数値計算法

2.1 数値スキーム

一般座標系 3 次元圧縮性 Navier-Stokes 方程式を支配方程式とし、有限差分法で解いた。方程式系を閉じるために、完全気体の状態方程式、粘度に対して Sutherland の公式、Prandtl 数として 0.72 を用いた。メトリクス、対流項および粘性項における空間微係数は、3 重対角システムの空間 6 次精度コンパクトスキーム [2] により評価した。境界近傍の扱いに関しては、境界上格子点において片側空間 4 次精度コンパクトスキーム [2] を、さらに、境界より 1 点内側の格子点において空間 4 次精度 classical Padé スキーム [2] を用いた。時間積分は 3 次精度陽的 Runge-Kutta 法により行った。これらの空間差分および時間積分に加えて、本計算では、コンパクトスキームの中心差分に伴う数値的不安定性を抑制するため、10 次精度の陰的フィルタリング操作 [3] を導入している。計算プログラムは Message Passing Interface(MPI) により並列化した。

2.2 非適合インターフェース条件

表面突起列を表現するため、特性線に基づくインターフェース条件を用いた。その基本的な方法は [4,5] で提案されているが、本研究に現れる非適合インターフェースを扱うために、理論の拡張を行う。基本的な方法ではまず、右領域（領域 R）および左領域（領域 L）のインターフェース上で保存量ベクトル Q_R および Q_L を以下の式に基づき求める。

$$\left.\frac{\partial Q}{\partial t}\right|_L = \left.(A_s^+)\right|_L \left.(RHS)\right|_L + \left.(A_s^-)\right|_L \left.(RHS)\right|_R, \qquad (1)$$

and

$$\left.\frac{\partial Q}{\partial t}\right|_R = \left.(A_s^+)\right|_R \left.(RHS)\right|_L + \left.(A_s^-)\right|_R \left.(RHS)\right|_R. \qquad (2)$$

次に、Q_R および Q_L を平均することにより、一意の保存量ベクトルを得る。

$$Q^* = \frac{1}{2}(Q_L + Q_R) \qquad (3)$$

ここで、数式 (1),(2) において、

$$RHS \equiv J(RHS_C + s \cdot RHS_V)$$
$$= J\left[-\left(\frac{\partial F}{\partial \xi} + \frac{\partial G}{\partial \eta} + \frac{\partial H}{\partial \zeta}\right) + s \cdot RHS_V\right] \quad (4)$$

$$A_s^- = P_{QV_C}\, diag\left(\frac{1 - sign(\lambda_i)}{2}\right) P_{QV_C}^{-1} \quad (5)$$

そして

$$A_s^+ = P_{QV_C}\, diag\left(\frac{1 + sign(\lambda_i)}{2}\right) P_{QV_C}^{-1} \quad (6)$$

である。

ここで、P_{QVC} は保存量ベクトル Q を特性量ベクトル Vc で偏微分して得られる 5 × 5 型の行列である。

$$P_{QV_C} \equiv \frac{\partial Q}{\partial V_C}. \quad (7)$$

λ_i(i=1,…,5) は以下のように定義される特性速度である。

$$\lambda_1 = \lambda_2 = \lambda_3 = \tilde{u}, \quad \lambda_4 = \tilde{u} + \tilde{a}, \quad \lambda_5 = \tilde{u} - \tilde{a} \quad (8)$$

反変速度 $\tilde{u}$ は

$$\tilde{u} \equiv \xi_x u + \xi_y v + \xi_z w \quad (9)$$

と定義され、メトリックでスケーリングされた音速 $\tilde{a}$ は

$$\tilde{a} \equiv a\sqrt{\xi_x^2 + \xi_y^2 + \xi_z^2}. \quad (10)$$

と定義される。

上述の方法は、インターフェース上で領域 R および L の格子点位置が一致していると仮定している。しかしながら、この研究では両領域からの格子点が一致しない状況が現れる。これに対処するため、上述の方法を非適合ケースに対して拡張する。

まず領域 L において、インターフェースの格子点上で $(RHS)_L$ を求める。この領域は、領域 R においてインターフェース上の格子点で求めた $(RHS)_R$ を受け取る。この $(RHS)_R$ は領域 L から見ると、同じインターフェース上にあっても異なる格子点で定義されているため、ラグランジュ補間により、領域 L におけるインターフェース格子点に補間する。インターフェースを通過する際の渦の歪みを避けるため、4 次の補間を利用した。ピッチ方向境界近くでは、補間精度を維持するため周期境界条件に則り格子点をピッチ方向にコピーして補間した。領域 R では、同様の方法を実施し、保存量ベクトルを更新した。

次に、Q_R^* および Q_L を平均することにより、一意の保存量ベクトルを得る。

$$Q^* = \frac{1}{2}(Q_L + Q_R^*) \quad (11)$$

領域 R では、同様の方法を実施し、保存量ベクトルを更新した。

3. シミュレーション結果

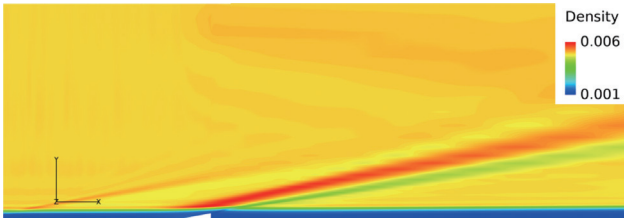

図 1　計算により求めた密度場（M_∞=6）、（楔状突起より衝撃波が発生している。）

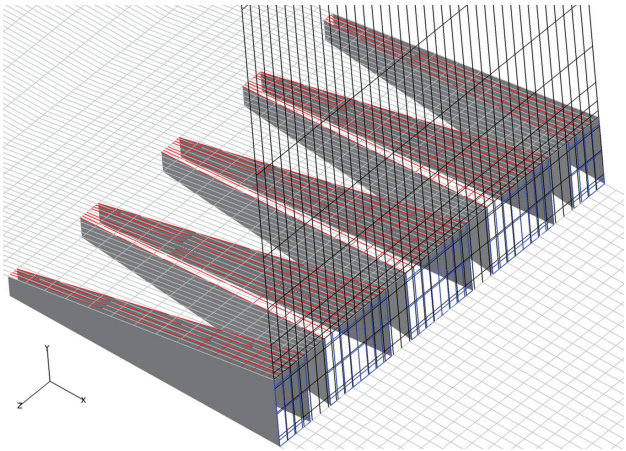

図 2　楔形突起列に対するインターフェース格子（各方向 5 格子線毎描いている。）

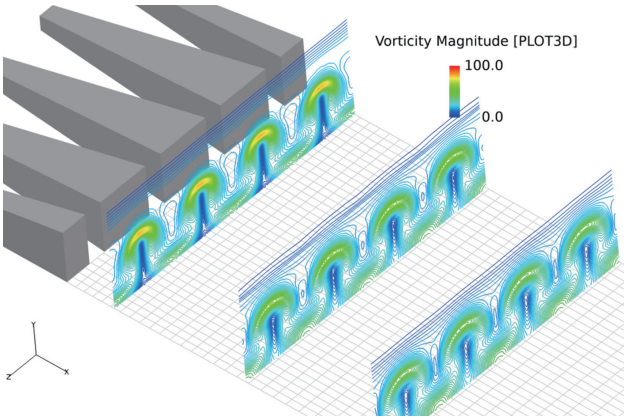

図 3　楔形突起列により生成された縦渦列

極超音速境界層における擾乱の空間発展に関して、数値計算に基づく研究を実施した。擾乱は楔状の表面突起列 [6] により生成した。本計算の実現に必要な非適合インターフェースにおける特性線に基づくインターフェース条件を開発することができた。その結果、マッハ 6 の境界層において縦渦列の空間発展を計算することができた。

4. 完全非線形安定性解析

導出した完全非線形擾乱方程式に関して、主流方向（x 方向）速度 u に関する式を示す。

$$\frac{\partial \tilde{u}}{\partial t}=\sum_{k=1}^{37}u_k,$$

$$u_1=-\bar{u}\frac{\partial \tilde{u}}{\partial x},\ u_2=-\tilde{u}\frac{\partial \bar{u}}{\partial x},\ u_3=-\bar{v}\frac{\partial \tilde{u}}{\partial y},$$

$$u_4=-\tilde{v}\frac{\partial \bar{u}}{\partial y},\ u_5=-\bar{w}\frac{\partial \tilde{u}}{\partial z},\ u_6=-\tilde{w}\frac{\partial \bar{u}}{\partial z},$$

$$u_7=-\frac{\tilde{\rho}}{\bar{\rho}}\bar{u}\frac{\partial \bar{u}}{\partial x},\ u_8=-\frac{\tilde{\rho}}{\bar{\rho}}\bar{v}\frac{\partial \bar{u}}{\partial y},\ u_9=-\frac{\tilde{\rho}}{\bar{\rho}}\bar{w}\frac{\partial \bar{u}}{\partial z},\ u_{10}=-\frac{1}{\bar{\rho}}(\frac{\partial \bar{p}}{\partial x})_L,$$

$$u_{11}=\frac{1}{\bar{\rho}\,\mathrm{Re}}\frac{\partial}{\partial x}[2\bar{\mu}\{-\frac{1}{3}(\nabla\cdot\tilde{\boldsymbol{u}})+\frac{\partial \tilde{u}}{\partial x}\}],$$

$$u_{12}=\frac{1}{\bar{\rho}\,\mathrm{Re}}\frac{\partial}{\partial y}\{\bar{\mu}(\frac{\partial \tilde{v}}{\partial x}+\frac{\partial \tilde{u}}{\partial y})\},\ u_{13}=\frac{1}{\bar{\rho}\,\mathrm{Re}}\frac{\partial}{\partial z}\{\bar{\mu}(\frac{\partial \tilde{u}}{\partial z}+\frac{\partial \tilde{w}}{\partial x})\},$$

$$u_{14}=-\bar{u}\frac{\partial \bar{u}}{\partial x},\ u_{15}=-\bar{v}\frac{\partial \bar{u}}{\partial y},\ u_{16}=-\bar{w}\frac{\partial \bar{u}}{\partial z},\ u_{17}=-\frac{1}{\bar{\rho}}\frac{\partial \bar{p}}{\partial x},$$

$$u_{18}=\frac{1}{\bar{\rho}\,\mathrm{Re}}\frac{\partial}{\partial x}[2\bar{\mu}\{-\frac{1}{3}(\nabla\cdot\bar{\boldsymbol{u}})+\frac{\partial \bar{u}}{\partial x}\}],$$

$$u_{19}=\frac{1}{\bar{\rho}\,\mathrm{Re}}\frac{\partial}{\partial y}\{\bar{\mu}(\frac{\partial \bar{v}}{\partial x}+\frac{\partial \bar{u}}{\partial y})\},\ u_{20}=\frac{1}{\bar{\rho}\,\mathrm{Re}}\frac{\partial}{\partial z}\{\bar{\mu}(\frac{\partial \bar{u}}{\partial z}+\frac{\partial \bar{w}}{\partial x})\},\qquad(12)$$

$$u_{21}=-\frac{\tilde{\rho}}{\bar{\rho}}\frac{\partial \tilde{u}}{\partial t},\ u_{22}=-\tilde{u}\frac{\partial \tilde{u}}{\partial x},\ u_{23}=-\tilde{v}\frac{\partial \tilde{u}}{\partial y},\ u_{24}=-\tilde{w}\frac{\partial \tilde{u}}{\partial z},$$

$$u_{25}=-\frac{\tilde{\rho}}{\bar{\rho}}\bar{u}\frac{\partial \tilde{u}}{\partial x},\ u_{26}=-\frac{\tilde{\rho}}{\bar{\rho}}\tilde{u}\frac{\partial \bar{u}}{\partial x},\ u_{27}=-\frac{\tilde{\rho}}{\bar{\rho}}\tilde{u}\frac{\partial \tilde{u}}{\partial x},$$

$$u_{28}=-\frac{\tilde{\rho}}{\bar{\rho}}\bar{v}\frac{\partial \tilde{u}}{\partial y},\ u_{29}=-\frac{\tilde{\rho}}{\bar{\rho}}\tilde{v}\frac{\partial \bar{u}}{\partial y},\ u_{30}=-\frac{\tilde{\rho}}{\bar{\rho}}\tilde{v}\frac{\partial \tilde{u}}{\partial y},$$

$$u_{31}=-\frac{\tilde{\rho}}{\bar{\rho}}\bar{w}\frac{\partial \tilde{u}}{\partial z},\ u_{32}=-\frac{\tilde{\rho}}{\bar{\rho}}\tilde{w}\frac{\partial \bar{u}}{\partial z},\ u_{33}=-\frac{\tilde{\rho}}{\bar{\rho}}\tilde{w}\frac{\partial \tilde{u}}{\partial z},$$

$$u_{34}=-\frac{1}{\bar{\rho}\gamma M^2}\frac{\partial}{\partial x}(\tilde{\rho}\tilde{T}),$$

$$u_{35}=\frac{1}{\bar{\rho}\,\mathrm{Re}}\frac{\partial}{\partial x}[2\tilde{\mu}\{-\frac{1}{3}(\nabla\cdot\bar{\boldsymbol{u}})-\frac{1}{3}(\nabla\cdot\tilde{\boldsymbol{u}})+\frac{\partial \bar{u}}{\partial x}+\frac{\partial \tilde{u}}{\partial x}\}],$$

$$u_{36}=\frac{1}{\bar{\rho}\,\mathrm{Re}}\frac{\partial}{\partial y}[\tilde{\mu}(\frac{\partial \bar{v}}{\partial x}+\frac{\partial \bar{u}}{\partial y}+\frac{\partial \tilde{v}}{\partial x}+\frac{\partial \tilde{u}}{\partial y})],$$

$$u_{37}=\frac{1}{\bar{\rho}\,\mathrm{Re}}\frac{\partial}{\partial z}[\tilde{\mu}(\frac{\partial \bar{u}}{\partial z}+\frac{\partial \bar{w}}{\partial x}+\frac{\partial \tilde{u}}{\partial z}+\frac{\partial \tilde{w}}{\partial x})]$$

ここで、ρ は密度、$\mathbf{u}=(u,v,w)$ は速度、T は温度、p は圧力、μ は粘度、Re はレイノルズ数、M はマッハ数、γ は比熱比をそれぞれ表す。上付き“-”はベース量、上付き“~”は擾乱、下添え字 L は線形項をそれぞれ表す。

謝辞

本研究は、科研費・基盤研究 (C) 15K04759 および住友財団・基礎科学研究助成の支援を受けた。ここに謝意を表する。

文献

[1] L.M. Mack, “Boundary layer linear stability theory: special course on stability and transition of laminar flow,” AGARD, Rep. 709, Paris, France 1984.

[2] S.K. Lele, “Compact finite difference schemes with spectral-like resolution,” J. Comput. Phys., Vol.103, No.1, pp.16-42, 1992.

[3] D.V. Gaitonde, M.R. Visbal, “Padé-type higher-order boundary filters for the Navier-Stokes equations,” AIAA J. Vol.38, No.11, pp.2103-2112, 2000.

[4] J.W. Kim, D.J. Lee, “Generalized characteristic boundary conditions for computational aeroacoustics, Part 2,” AIAA J., Vol.42, No.1, pp.47-55, 2004.

[5] X. Deng, et al., “Extending the fifth-order weighted compact nonlinear scheme to complex grids with characteristic-based interface conditions,” AIAA J., Vol.48, No.12, pp.2840-2851, 2010.

[6] S. Berry, et al., “Boundary-layer transition on X-43A”, J. Spacecraft & Rockets, Vol.47, No.6, pp.922-934, 2010.

Overall Simulation of Nonlinear Vortex Dynamics in Compressible Transitional Boundary Layers

Project Representative
Kazuo Matsuura Ehime University, Graduate school of science and engineering

Author
Kazuo Matsuura Ehime University, Graduate school of science and engineering

The Mach number at the edge of the boundary layer Me is known to have a great influence on the stability of the laminar boundary layer. Above $Me \geq 4$, the stability of the boundary layer is drastically enhanced as Mach number is increased. Theories of linear stability, secondary instability, non-linear parabolic stability equation, transient growth are fairly successful in predicting the growth of disturbances locally or globally. However, there are still gaps between the stability theories and ways to become turbulence. Direct numerical simulation (DNS) can analyze the Navier-Stokes equations faithfully if initial and condition, boundary condition, computational mesh and time increment are given properly. In this study, it is aimed to conduct DNSs in which disturbances that are considered to make boundary layer unstable easily are introduced to the boundary layer, and numerical techniques necessary to realize such simulation are developed.

Keywords: Hypersonic flow, laminar-turbulent transition, roughness, direct numerical simulation, interface condition

1. Introduction

When a flow encounters a solid object, a boundary layer is formed near the solid surface. Although the boundary layer is initially laminar, laminar-turbulent transition takes place at some downstream. The routes of transition are never single nor simple, and multiple routes exist depending on mean flow and interior and/or exterior disturbances. Underlying instability mechanism which determines what disturbances are amplified, sometimes as a result of competition, also differs depending on the routes.

The Mach number at the edge of the boundary layer Me is known to have a great influence on the stability of the laminar boundary layer. Above $Me \geq 4$, the stability of the boundary layer is drastically enhanced as Mach number is increased. As Mack showed [1], there are higher acoustic instability modes with higher frequencies in supersonic or hypersonic boundary layers in addition to the first instability mode corresponding to Tollmien-Schlichting waves in low-speed flows. The two-dimensional second Mack mode dominates in hypersonic boundary layer in contrast to the unstable oblique first mode in low-speed boundary layer flow.

Theories of linear stability, secondary instability, non-linear parabolic stability equation, transient growth are fairly successful in predicting the growth of disturbances locally or globally. However, there are still gaps between the stability theories and ways to become turbulence. Direct numerical simulation (DNS) can analyze the Navier-Stokes equations faithfully if initial and condition, boundary condition, computational mesh and time increment are given properly.

In this study, it is aimed at to conduct a numerical simulation in which disturbances that are considered to make boundary layer unstable easily are introduced to the boundary layer, and numerical techniques necessary to realize such simulation is developed. In this year, a non-conforming characteristic interface condition and a numerical simulation of introducing streamwise vortices by an array of wedge-shaped roughness under Mach 6 are conducted.

2. Numerical Method

2.1 Numerical scheme

The governing equations are the unsteady three-dimensional fully compressible Navier-Stokes equations in general coordinates (ξ, η, ζ). The perfect gas law closes the system of equations. Viscosity is evaluated by Sutherland's formula and a constant Prandtl number of Pr=0.72 is assumed. The equations are solved using the finite-difference method. Spatial derivatives that appear in the metrics, convective and viscous terms are evaluated using the sixth-order tridiagonal compact scheme [2]. Near boundaries, the fourth-order one-sided and classical Padé schemes are used on the boundaries and at one point internal to them. Time-dependent solutions to the governing equations are obtained using the third-order explicit Runge-Kutta scheme. In addition to the above-mentioned spatial discretization and time integration, a tenth-order implicit filtering [3] is introduced to suppress numerical instabilities that arise from central differencing in the compact scheme. The computational program is parallelized by Message Passing Interface (MPI).

2.2 Non-Conforming Interface Condition

In order to represent the array of roughness, a characteristic

interface condition is used. While its baseline method is proposed in [4,5], we extend it for the non-conforming situation we encounter in this study. In the baseline method, first the vectors of conservative variables Q_R and Q_L are evaluated on the interface of the right (R) and left (L) regions, respectively by integrating the following equations.

$$\left.\frac{\partial Q}{\partial t}\right|_L = \left(A_s^+\right)\Big|_L (RHS)\Big|_L + \left(A_s^-\right)\Big|_L (RHS)\Big|_R, \quad (1)$$

and

$$\left.\frac{\partial Q}{\partial t}\right|_R = \left(A_s^+\right)\Big|_R (RHS)\Big|_L + \left(A_s^-\right)\Big|_R (RHS)\Big|_R. \quad (2)$$

Secondary, a unique vector of the conservative variables is obtained by averaging Q_R and Q_L, i.e.,

$$Q^* = \frac{1}{2}(Q_L + Q_R) \quad (3)$$

In eqs.(1,2),

$$RHS \equiv J(RHS_C + s \cdot RHS_V) = J\left[-\left(\frac{\partial F}{\partial \xi} + \frac{\partial G}{\partial \eta} + \frac{\partial H}{\partial \zeta}\right) + s \cdot RHS_V\right] \quad (4)$$

$$A_s^- = P_{QV_C}\, diag\left(\frac{1 - sign(\lambda_i)}{2}\right) P_{QV_C}^{-1} \quad (5)$$

and

$$A_s^+ = P_{QV_C}\, diag\left(\frac{1 + sign(\lambda_i)}{2}\right) P_{QV_C}^{-1} \quad (6)$$

Here, P_{QVC} is a 5×5 matrix obtained by partially differentiating a vector of the conservative variables Q by a vector of the characteristic variables, i.e.,

$$P_{QV_C} \equiv \frac{\partial Q}{\partial V_C}. \quad (7)$$

λi(i=1,…,5) are the characteristic speeds, defined as

$$\lambda_1 = \lambda_2 = \lambda_3 = \tilde{u}, \quad \lambda_4 = \tilde{u} + \tilde{a}, \quad \lambda_5 = \tilde{u} - \tilde{a} \quad (8)$$

using the contravariant velocity $\tilde{u}$ defined as

$$\tilde{u} \equiv \xi_x u + \xi_y v + \xi_z w \quad (9)$$

and the sound speed $\tilde{a}$ scaled by metrics, which is defined as

$$\tilde{a} \equiv a\sqrt{\xi_x^2 + \xi_y^2 + \xi_z^2}. \quad (10)$$

The above discussion assumes the location of mesh points from both of the regions R and L coincide at the interface. However, in this study, the mesh points from both of the regions do not match. In order to cope with this situation, the above method is extended for the non-conforming case.

The L region first evaluates $(RHS)_L$ at the mesh points on the interface. The region receives $(RHS)_R$, which are evaluated at the mesh points on the interface in the right region. The $(RHS)_R$ are interpolated onto the mesh points on the interface in the L left region by the Lagrange interpolation. The 4th order interpolation is used to prevent the deformation of vortices passing through the interface. Near the pitchwise boundaries, the order of the interpolation, i.e., the fixed number of donar points is assured by copying the R region periodically in the pitchwise direction. In the R region, similar operations are conducted and the vector of conservative variables is updated.

Secondly, a unique vector of conservative variables is obtained by averaging Q^*_R and Q_L in the L region, i.e.,

$$Q^* = \frac{1}{2}(Q_L + Q_R^*) \quad (11)$$

In the R region, similar operations are conducted and the vector of conservative variables is updated.

3. Results

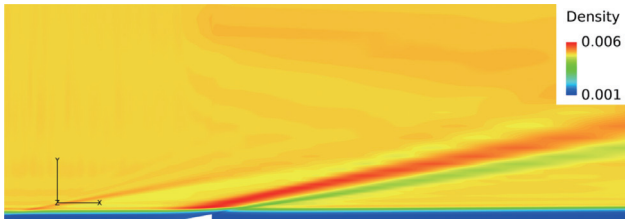

Fig. 1 Computed density field ($M\infty$=6), Shock waves are generated from the roughness

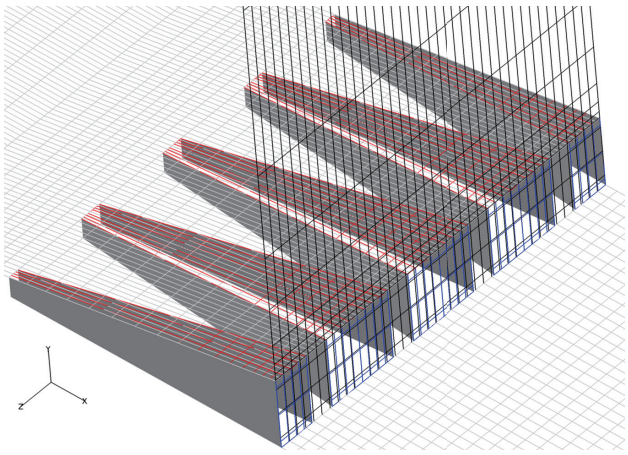

Fig. 2 Mesh interface for the array of the wedge-shaped (every 5 grid lines are drawn in all the directions)

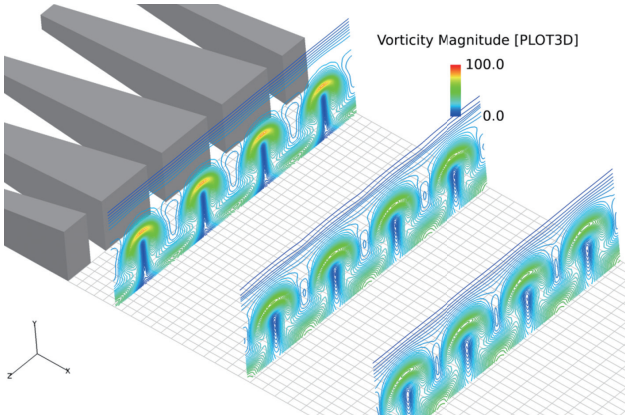

Fig. 3 Generation of the array of streamwise vortices by the array of the wedge-shaped roughness

Numerical computations of disturbance evolution in hypersonic boundary layers are conducted. The disturbances are generated by the array of the wedge-shaped roughness [6]. Computational technique necessary for realizing the simulations are also developed. Non-conforming interface based on the characteristic interface condition is developed. Evolution of the array of streamwise vortices is computed for the boundary layer flow at Mach 6.

4. Fully-Nonlinear Disturbance Analysis

Fully-nonlinear disturbance equation for the streamwise velocity u is shown.

$$\frac{\partial \tilde{u}}{\partial t}=\sum_{k=1}^{37}u_k,$$

$$u_1=-\bar{u}\frac{\partial \tilde{u}}{\partial x},\ u_2=-\tilde{u}\frac{\partial \bar{u}}{\partial x},\ u_3=-\bar{v}\frac{\partial \tilde{u}}{\partial y},$$

$$u_4=-\tilde{v}\frac{\partial \bar{u}}{\partial y},\ u_5=-\bar{w}\frac{\partial \tilde{u}}{\partial z},\ u_6=-\tilde{w}\frac{\partial \bar{u}}{\partial z},$$

$$u_7=-\frac{\tilde{\rho}}{\bar{\rho}}\bar{u}\frac{\partial \bar{u}}{\partial x},\ u_8=-\frac{\tilde{\rho}}{\bar{\rho}}\bar{v}\frac{\partial \bar{u}}{\partial y},\ u_9=-\frac{\tilde{\rho}}{\bar{\rho}}\bar{w}\frac{\partial \bar{u}}{\partial z},\ u_{10}=-\frac{1}{\bar{\rho}}(\frac{\partial \tilde{p}}{\partial x})_L,$$

$$u_{11}=\frac{1}{\bar{\rho}\,\mathrm{Re}}\frac{\partial}{\partial x}[2\bar{\mu}\{-\frac{1}{3}(\nabla\cdot\tilde{\boldsymbol{u}})+\frac{\partial \tilde{u}}{\partial x}\}],$$

$$u_{12}=\frac{1}{\bar{\rho}\,\mathrm{Re}}\frac{\partial}{\partial y}\{\bar{\mu}(\frac{\partial \tilde{v}}{\partial x}+\frac{\partial \tilde{u}}{\partial y})\},\ u_{13}=\frac{1}{\bar{\rho}\,\mathrm{Re}}\frac{\partial}{\partial z}\{\bar{\mu}(\frac{\partial \tilde{u}}{\partial z}+\frac{\partial \tilde{w}}{\partial x})\},$$

$$u_{14}=-\bar{u}\frac{\partial \bar{u}}{\partial x},\ u_{15}=-\bar{v}\frac{\partial \bar{u}}{\partial y},\ u_{16}=-\bar{w}\frac{\partial \bar{u}}{\partial z},\ u_{17}=-\frac{1}{\bar{\rho}}\frac{\partial \bar{p}}{\partial x},$$

$$u_{18}=\frac{1}{\bar{\rho}\,\mathrm{Re}}\frac{\partial}{\partial x}[2\bar{\mu}\{-\frac{1}{3}(\nabla\cdot\bar{\boldsymbol{u}})+\frac{\partial \bar{u}}{\partial x}\}],$$

$$u_{19}=\frac{1}{\bar{\rho}\,\mathrm{Re}}\frac{\partial}{\partial y}\{\bar{\mu}(\frac{\partial \bar{v}}{\partial x}+\frac{\partial \bar{u}}{\partial y})\},\ u_{20}=\frac{1}{\bar{\rho}\,\mathrm{Re}}\frac{\partial}{\partial z}\{\bar{\mu}(\frac{\partial \bar{u}}{\partial z}+\frac{\partial \bar{w}}{\partial x})\},\qquad(12)$$

$$u_{21}=-\frac{\tilde{\rho}}{\bar{\rho}}\frac{\partial \tilde{u}}{\partial t},\ u_{22}=-\tilde{u}\frac{\partial \tilde{u}}{\partial x},\ u_{23}=-\tilde{v}\frac{\partial \tilde{u}}{\partial y},\ u_{24}=-\tilde{w}\frac{\partial \tilde{u}}{\partial z},$$

$$u_{25}=-\frac{\tilde{\rho}}{\bar{\rho}}\bar{u}\frac{\partial \tilde{u}}{\partial x},\ u_{26}=-\frac{\tilde{\rho}}{\bar{\rho}}\tilde{u}\frac{\partial \bar{u}}{\partial x},\ u_{27}=-\frac{\tilde{\rho}}{\bar{\rho}}\tilde{u}\frac{\partial \tilde{u}}{\partial x},$$

$$u_{28}=-\frac{\tilde{\rho}}{\bar{\rho}}\bar{v}\frac{\partial \tilde{u}}{\partial y},\ u_{29}=-\frac{\tilde{\rho}}{\bar{\rho}}\tilde{v}\frac{\partial \bar{u}}{\partial y},\ u_{30}=-\frac{\tilde{\rho}}{\bar{\rho}}\tilde{v}\frac{\partial \tilde{u}}{\partial y},$$

$$u_{31}=-\frac{\tilde{\rho}}{\bar{\rho}}\bar{w}\frac{\partial \tilde{u}}{\partial z},\ u_{32}=-\frac{\tilde{\rho}}{\bar{\rho}}\tilde{w}\frac{\partial \bar{u}}{\partial z},\ u_{33}=-\frac{\tilde{\rho}}{\bar{\rho}}\tilde{w}\frac{\partial \tilde{u}}{\partial z},$$

$$u_{34}=-\frac{1}{\bar{\rho}\gamma M^2}\frac{\partial}{\partial x}(\tilde{\rho}\tilde{T}),$$

$$u_{35}=\frac{1}{\bar{\rho}\,\mathrm{Re}}\frac{\partial}{\partial x}[2\tilde{\mu}\{-\frac{1}{3}(\nabla\cdot\bar{\boldsymbol{u}})-\frac{1}{3}(\nabla\cdot\tilde{\boldsymbol{u}})+\frac{\partial \bar{u}}{\partial x}+\frac{\partial \tilde{u}}{\partial x}\}],$$

$$u_{36}=\frac{1}{\bar{\rho}\,\mathrm{Re}}\frac{\partial}{\partial y}[\tilde{\mu}(\frac{\partial \bar{v}}{\partial x}+\frac{\partial \bar{u}}{\partial y}+\frac{\partial \tilde{v}}{\partial x}+\frac{\partial \tilde{u}}{\partial y})],$$

$$u_{37}=\frac{1}{\bar{\rho}\,\mathrm{Re}}\frac{\partial}{\partial z}[\tilde{\mu}(\frac{\partial \bar{u}}{\partial z}+\frac{\partial \bar{w}}{\partial x}+\frac{\partial \tilde{u}}{\partial z}+\frac{\partial \tilde{w}}{\partial x})]$$

Here ρ is density, $\mathbf{u}=(u, v, w)$ is velocity, T is temperature, p is pressure, μ is viscosity, Re is Reynolds number, M is Mach number γ is heat ratio, respectively. Overbar "-" is a base quantity, tilde "~" is fluctuation, subscript "L" is a linter term, respectively.

Acknowledgement

This work was financially supported by the Ministry of Education, Culture, Sports, Science and Technology (MEXT) through a Grant-in-Aid for Scientific Research (C), 15K04759, 2015, and Grant for Basic Science Research Projects from the Sumitomo Foundation.

References

[1] L.M. Mack, "Boundary layer linear stability theory: special course on stability and transition of laminar flow," AGARD, Rep. 709, Paris, France 1984.

[2] S.K. Lele, "Compact finite difference schemes with spectral-like resolution," J. Comput. Phys., Vol.103, No.1, pp.16-42, 1992.

[3] D.V. Gaitonde, M.R. Visbal, "Padé-type higher-order boundary filters for the Navier-Stokes equations," AIAA J. Vol.38, No.11, pp.2103-2112, 2000.

[4] J.W. Kim, D.J. Lee, "Generalized characteristic boundary conditions for computational aeroacoustics, Part 2," AIAA J., Vol.42, No.1, pp.47-55, 2004.

[5] X. Deng, et al., "Extending the fifth-order weighted compact nonlinear scheme to complex grids with characteristic-based interface conditions," AIAA J., Vol.48, No.12, pp.2840-2851, 2010.

[6] S. Berry, et al., "Boundary-layer transition on X-43A", J. Spacecraft & Rockets, Vol.47, No.6, pp.922-934, 2010.